

Long Time Computation of Two-Dimensional Vortex Sheet by Point Vortex Method

Sun-Chul KIM, June-Yub LEE¹ and Sung-Ik SOHN²

Department of Mathematics, Chung-Ang University, Seoul 156-756, Korea

¹*Department of Mathematics, Ewha women's University, Seoul 120-750, Korea*

²*School of Information Engineering, Tongmyong University of IT, Pusan 608-711, Korea*

(Received March 17, 2003)

Two-dimensional vortex sheet suffers an unstable deformation from the Kelvin–Helmholtz instability and a curvature singularity which develops in a finite time. In this paper, long time computations of the two-dimensional vortex sheet are performed by a robust and efficient numerical method with high accuracy. To handle the rapid and non-uniform stretching of the interface, we adopt the adaptive point insertion and redistribution procedures. Computational results show highly refined structures of a complex and chaotic pattern for the vortex sheet up to very long time.

KEYWORDS: vortex sheet, Kelvin–Helmholtz instability, point vortex method, singularity, redistribution
DOI: 10.1143/JPSJ.72.1968

1. Introduction

A periodically perturbed vortex sheet is a simple model for the instability of a parallel shear flow to streamwise perturbations. In this model, the transition region between the two streams is approximated by a surface across which the tangential velocity is discontinuous. This vortex sheet has drawn a lot of attention ever since Birkhoff.⁴⁾ Asymptotic analysis and numerical results show that a singularity forms in the vortex sheet at a finite time.^{4,9,15)} Due to the singularity from Kelvin–Helmholtz instability, numerical simulations for the vortex sheet have significant difficulties. In this paper, we present long time simulations for the vortex sheet in two dimensions by a robust point vortex method.

In the point vortex method, the vortex sheet is considered as a set of point vortices which are computed in Lagrangian manner. To deal with the singularity and instability of the vortex sheet, point vortices are usually regularized by vortices with finite cores or “blobs” of vorticity. This type of desingularization method was originally introduced by Chorin and Bernard⁶⁾ and successfully applied to the vortex sheet by Krasny.¹⁰⁾ Recent studies on the vortex sheet can be found in literature^{2,5,8,13,14,17)} and traced by the references therein.

Although the vortex sheet has been extensively studied for last decades, long time structures of the vortex sheet are not thoroughly investigated yet, due to complex or chaotic pattern as well as heavy computations. The complex pattern in long time was first predicted by Krasny.¹¹⁾ Recently, Sakajo and Okamoto¹⁷⁾ applied a fast algorithm to simulate the long time evolution of vortex sheet. Although the result¹⁷⁾ gives the overall correct description for the vortex sheet, it does not provide the fine structure for chaotic patterns around the core part of vortex sheet. This low resolution is possibly due to the approximations in the fast algorithm and the unsymmetric kernel used in the vortex method.

Main objects of this paper are to present a robust and efficient numerical method with high accuracy and to provide highly resolved solutions of the vortex sheet in long time. The direct implementation for governing equations of the vortex sheet uses fixed number of vortex blobs uniformly spaced with respect to the circulation parameter.

However, for long time simulations, computations under the uniform discretization with fixed number of vortices can not proceed at some finite time because distances between neighboring point vortices become too large to resolve the vortex sheet and eventually the curve is tangled. [See Fig. 5(a).] Numerical results show rapid stretching and non-uniform elongation of the vortex sheet. In fact, vortex blobs around the center of the sheet tend to cluster, and vortex blobs near the end points of the sheet diverge as time proceeds. (See Fig. 4.) In addition, the inherent singularity and instability of the sheet make long time computations seriously difficult.

Computational efficiency is another key factor in the vortex method. The computation cost of the point vortex method is order of N^2 where N is the number of point vortices. Therefore, if we increase the number of point vortices to resolve the vortex sheet, the computation cost grows drastically. The numerical method for long time simulations of the vortex sheet should be designed to perform computations within reasonable finite time.

Several approaches have been applied to overcome these troubles. One of such efforts is to distribute, initially, the vortex blobs non-uniformly. Sakajo and Okamoto¹⁷⁾ used fixed number of blobs which are densely placed around two end points and coarsely around the center of the sheet by an appropriate transformation. This method is adequate to deal with stretching near the two ends, but it can not handle dynamic non-uniform elongations along the vortex sheet. Therefore, the number of blobs should be large enough to resolve the long time vortex sheet, which leads to heavy computations.

More efficient approach is the redistribution method in which vortex blobs are relocated at every or certain time steps. One of the earliest redistribution methods is proposed by Fink and Soh,⁷⁾ which uses two family of points, pivotal points and segmental points. We applied Fink and Soh's method to our problem and found that it was not effective for long time simulation for vortex sheet. See also comments in Baker.¹⁾ Moore presented a different redistribution method based on Legendre polynomials, interpolating neighboring three points.¹⁶⁾ The vortex points were evenly distributed with respect to arc-length. Moore's method provides a simple algorithm for the vortex sheet, but it is not accurate

enough for simulations of highly distorted and complex curves of the long time vortex sheet.

Another possible approach is a point insertion technique, which is first presented by Krasny^{11,12)} for the long time simulation of vortex sheet. At every time step, if the distance of two adjacent points is larger than a given tolerance, a new point is inserted by a local cubic polynomial in terms of the circulation parameter interpolating neighboring points. Krasny's method is appropriate for computations of stretched vortex sheet, but it can not effectively handle node clustering around the center as the initial vortex points are kept.

We develop a vortex method which efficiently deals with the problems for the long time vortex sheet stated above. We adopt the redistribution method for particle points by the following rule: if the maximum distance of two adjacent points is larger than a given threshold constant, vortex points are redistributed. The key point of our method is that vortex points are redistributed uniformly in terms of the average of relative arc-length and circulation. This redistribution technique provides stable computations for the highly distorted vortex sheet and detailed discussions for the choice of redistribution parameter will be given in §3.

Simultaneously, we apply a point insertion technique to handle the stretching of the sheet. In our method, the point insertion is implemented only when the redistribution is necessary. The vortex sheet is first defined by a globally interpolated cubic spline, and then discretized uniformly with respect to our redistribution parameter using more vortex points. This redistribution procedure with point insertion suppresses the concentration or the divergence of point vortices, and therefore are more stable and computationally efficient than Krasny's direct point insertion method.^{11,13)}

The paper is organized as follows. Section 2 gives the numerical method for governing equations. Section 3 describes the procedures of point insertion and redistribution. The computational results are presented at §4. Section 5 gives the discussions and conclusive remarks.

2. Numerical Method for Desingularized Equations

A vortex sheet is a mathematical limit of a parallel shear flow where the fluid is irrotational everywhere except on the sheet.⁴⁾ In two dimensions, the vortex-sheet can be described by a curve $(x(\Gamma, t), y(\Gamma, t))$ where Γ is a circulation parameter measured from the origin and t is time, and is governed by the Birkhoff–Rott equation:

$$\begin{aligned} \frac{\partial z^*}{\partial t}(\Gamma, t) &= \frac{i}{2\pi} \text{p.v.} \int_{-\infty}^{\infty} \frac{1}{z(\Gamma', t) - z(\Gamma, t)} d\Gamma' \\ &= \frac{i}{2} \text{p.v.} \int_0^1 \cot(\pi(z' - z)) d\Gamma' \end{aligned} \quad (1)$$

in complex notation $z = x + yi$, $i = \sqrt{-1}$, with periodicity $z(\Gamma+1, t) = z(\Gamma, t) + 1$ where the asterisk represents the complex conjugate, p.v. the Cauchy principal value of integral, and $z' = z(\Gamma', t)$.

We consider a flat vortex sheet of constant strength given by $x(\Gamma, t) = \Gamma$, $y(\Gamma, t) = 0$ and perturb this equilibrium solution by a small sine oscillation

$$\begin{aligned} x(\Gamma, 0) &= \Gamma + 0.01 \sin(2\pi\Gamma), \\ y(\Gamma, 0) &= -0.01 \sin(2\pi\Gamma). \end{aligned} \quad (2)$$

It is known that the sheet with the initial data (2) develops a singularity in curvature at the center, $\Gamma = 0.5$, near $t \sim 0.375$ and is not analytic thereafter.^{15,18)} This produces a difficulty in numerical computation. Therefore, introducing the desingularizing parameter $\delta > 0$, we consider the “ δ -equations”

$$\frac{\partial x}{\partial t} = -\frac{1}{2} \int_0^1 \frac{\sinh 2\pi(y - y')}{\cosh 2\pi(y - y') - \cos 2\pi(x - x') + \delta^2} d\Gamma', \quad (3)$$

$$\frac{\partial y}{\partial t} = \frac{1}{2} \int_0^1 \frac{\sin 2\pi(x - x')}{\cosh 2\pi(y - y') - \cos 2\pi(x - x') + \delta^2} d\Gamma'. \quad (4)$$

Various forms of desingularized kernel in the integrals were studied.³⁾

As suggested,¹⁷⁾ the computation cost is greatly reduced by a transformation of the variable. We take the transformation $w = \exp(2\pi iz)$. Then, the functions in the integral (3) and (4) can be written as

$$\begin{aligned} \sinh 2\pi(y - y') &= \frac{1}{2} \left(\frac{|v|}{|w|} - \frac{|w|}{|v|} \right), \\ \sin 2\pi(x - x') &= \frac{1}{2i} \frac{|v|}{|w|} \left(\frac{w}{v} - \frac{w^*}{v^*} \right), \\ \cosh 2\pi(y - y') &= \frac{1}{2} \left(\frac{|v|}{|w|} + \frac{|w|}{|v|} \right), \\ \cos 2\pi(x - x') &= \frac{1}{2} \frac{|v|}{|w|} \left(\frac{w}{v} + \frac{w^*}{v^*} \right). \end{aligned}$$

where $v = \exp(2\pi iz')$. From these relations and $w = \exp(2\pi iz)$, we obtain

$$\frac{\partial w^*}{\partial t}(t, \Gamma) = \int_0^1 K_\delta(w(t, \Gamma), w(t, \Gamma')) d\Gamma' \quad (5)$$

where

$$K_\delta(w, v) = -\pi i w^* \frac{(w + v)(w^* - v^*)}{|w - v|^2 + 2\delta^2 |w||v|}. \quad (6)$$

Note that the kernel (6) is different from that in Sakajo and Okamoto.¹⁷⁾ As derived, (6) is the exact transformation for Krasny's desingularized kernel (3) and (4), which corresponds to a symmetric and smoothing cut-off function of the original one.

The curve $(x(\Gamma, t), y(\Gamma, t))$ is approximated by a finite number of points, $(x_j(t), y_j(t)) \approx (x(\Gamma_j, t), y(\Gamma_j, t))$, where $\Gamma_j = \frac{j}{N}$, $j = 0, \dots, N$. Then, we apply the trapezoidal rule to eq. (5) using the transformed point vortices $w_j(t) = \exp(2\pi iz_j(t))$ for $j = 0, \dots, N$ and obtain a system of ordinary differential equations for $w_j(t)$

$$\frac{dw_j^*}{dt}(t) = \frac{1}{N} \sum_{k=1}^N K_\delta(w_j(t), w_k(t)) \quad \text{for } j = 1, \dots, N. \quad (7)$$

The system (7) is solved by the classical fourth order Runge–Kutta method. After each Runge–Kutta time marching step for $\{w_j(t)\}$, the vortex points $\{z_j(t)\}$ are obtained by the inverse transformation from $\{w_j(t)\}$. The convergence of point vortex methods to weak solutions of the incompressible Euler equations, as $N \rightarrow \infty$ and $\delta \rightarrow 0$, even after the

formation of singularity, was proved by Liu and Xin.¹⁴⁾

To suppress the instability from the growth of round-off errors, we apply the Fourier filtering technique, which is introduced by Krasny.¹⁰⁾ That is to say, after each Runge–Kutta time marching step, we take the Fourier sine transformation for $\{x_j(t)\}$ and $\{y_j(t)\}$ and cut off high frequency modes whose amplitude is less than a given threshold, denoted as τ . For better resolution, the filter level τ needs to be reduced. We set the filter level to $\tau = 10^{-10}$, which gives enough resolution for solutions in all cases of our computations.

Figure 1 shows the numerical result of vortex sheet with $\delta = 0.3$ at $t = 5$ computed with time marching step $\Delta t = \frac{1}{240}$ and 12288 point vortices. Two periods of the vortex sheet are plotted in Fig. 1.

To determine the accuracy of the numerical scheme in space and in time, we plot the root mean square errors of numerical solution ($x_j(t = 5), y_j(t = 5)$) with various combinations of time step size $\Delta t = \frac{1}{5}, \frac{1}{10}, \frac{1}{15}, \frac{1}{20}, \frac{1}{30}, \frac{1}{40}, \frac{1}{60}, \frac{1}{80}, \frac{1}{160}$ and number of discretization points $N = 1024, 2048, 4096, 8192$ compared to that with $\Delta t = \frac{1}{240}$ and $N = 12288$ in Fig. 2. In other words, errors in Fig. 2 are defined as

$$E_{N,\Delta t} = \sqrt{\frac{1}{N} \sum_{j=1}^N [z_j^{N,\Delta t}(t = 5) - z_{j^*}^{N^*,\Delta t^*}(t = 5)]^2}$$

where j^* is the corresponding point index for j and $z_j^{N,\Delta t}(t = 5)$ is the numerical solution z_j at time $t = 5$ using the given parameters N and Δt , and N^* and Δt^* are fixed to 12288 and $\frac{1}{240}$, respectively. Figure 2 shows that, as time step decreases,

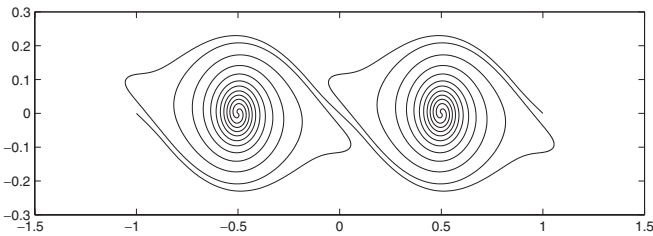


Fig. 1. Vortex sheet at $t = 5$ with $\delta = 0.3$. The number of discretization points are fixed to $N = 12288$.

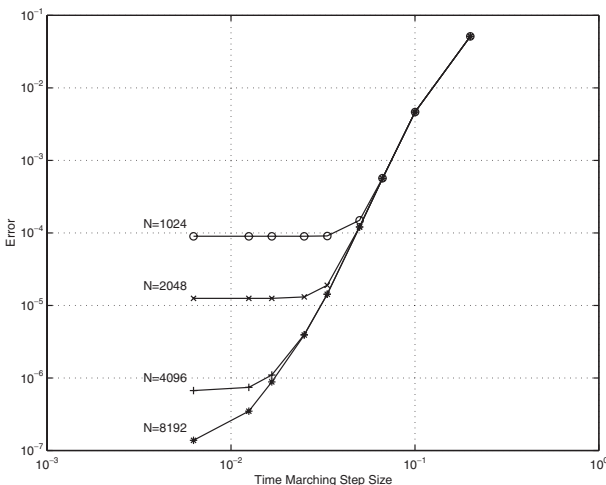


Fig. 2. Numerical errors at $t = 5$ with $\delta = 0.3$ as a function of marching step Δt for various number of discretization points N

so does the error until it is reduced to the level of the spatial discretization error limit by the trapezoidal rule used in computing the integral for $w_j(t)$. One can find from Fig. 2 that the Runge–Kutta method and the trapezoidal rule with the Fourier filtering for the transformed δ -equation (5) provides a fourth order accuracy in time and second order in space, respectively. Figure 2 also implies that, to enhance the resolution, two parameters N and Δt should be adjusted simultaneously. Fixing one parameter and only increasing/reducing the other parameter may not be effective in reducing errors.

3. Point Insertion and Redistribution Procedure

In this section, we present the point insertion and redistribution procedure for long time computation of the vortex sheet. The procedure in this section is implemented with the numerical method of §2.

We give an outline of our procedure of point insertion and redistribution. During the computation, rapidly increasing number of points are required to resolve the vortex sheet, since the arc-length is exponentially increasing with time. Therefore, at each time step we monitor the maximum distance between neighboring vortex points, Δs_{\max} , and if this value exceeds a given threshold, Δs_{lim} , then we apply the following steps:

- Step 1** Construct the periodic cubic splines for x and y .
- Step 2** Calculate the arc-length, $s(\Gamma, t)$, $0 \leq \Gamma \leq 1$, from the cubic splines in Step 1.
- Step 3** Introducing the new parameter p as $p(\Gamma, t) = \frac{1}{2} \left(\frac{s(\Gamma, t)}{s(1, t)} + \Gamma \right)$, construct the periodic cubic splines for p and Γ .
- Step 4** Increase the number of points N by a suitable strategy.
- Step 5** Evaluate the evenly spaced points $z_j = (x_j, y_j)$, $j = 0, \dots, N$, on the spline with respect to p and compute Γ_j on the new points z_j .

We now present each step in detail. In Step 1, we interpolate $\{x_j\}$ and $\{y_j\}$ defined on intervals between integer points $j = 0, \dots, N$ by cubic splines. We denote these splines as

$$q_{xj}(\lambda) = a_{xj} + b_{xj}(\lambda - j) + c_{xj}(\lambda - j)^2 + d_{xj}(\lambda - j)^3, \quad (8)$$

$$q_{yj}(\lambda) = a_{yj} + b_{yj}(\lambda - j) + c_{yj}(\lambda - j)^2 + d_{yj}(\lambda - j)^3 \quad (9)$$

for $\lambda \in [j, j + 1]$ and $j = 0, \dots, N - 1$. Note that $a_{xj} = x_j - \frac{j}{N}$, from periodicity, and $a_{yj} = y_j$. Second order Legendre polynomials,¹⁶⁾ involving a local construction, may be applied for the interpolation but have low order of accuracy. For long time computations, we choose the cubic splines with periodic boundary condition for higher order of accuracy.

In Step 2, we measure the arc-length of the vortex sheet from

$$s_{j+1}(t) = s_j(t) + \int_j^{j+1} \left| \frac{dz}{d\lambda} \right| d\lambda \quad (10)$$

with $s_0 = 0$. An accurate evaluation for the arc-length are critical in the long computation of the vortex sheet. Substituting (8) and (9) and applying Taylor series and composite Simpson’s rule of quadrature, the integral in (10) is approximated by

$$\begin{aligned}
 \int_j^{j+1} \left| \frac{dz}{d\lambda} \right| d\lambda &\approx \frac{1}{12} \sqrt{\tilde{b}_{xj}^2 + b_{yj}^2} \\
 &+ \frac{1}{3} \sqrt{\left(\tilde{b}_{xj} + \frac{1}{2} c_{xj} + \frac{3}{16} d_{xj} \right)^2 + \left(b_{yj} + \frac{1}{2} c_{yj} + \frac{3}{16} d_{yj} \right)^2} \\
 &+ \frac{1}{6} \sqrt{\left(\tilde{b}_{xj} + c_{xj} + \frac{3}{4} d_{xj} \right)^2 + \left(b_{yj} + c_{yj} + \frac{3}{4} d_{yj} \right)^2} \\
 &+ \frac{1}{3} \sqrt{\left(\tilde{b}_{xj} + \frac{3}{2} c_{xj} + \frac{27}{16} d_{xj} \right)^2 + \left(b_{yj} + \frac{3}{2} c_{yj} + \frac{27}{16} d_{yj} \right)^2} \\
 &+ \frac{1}{12} \sqrt{(\tilde{b}_{xj} + 2c_{xj} + 3d_{xj})^2 + (b_{yj} + 2c_{yj} + 3d_{yj})^2} \tag{11}
 \end{aligned}$$

where $\tilde{b}_{xj} = b_{xj} + 1/N$.

In Step 3, new parameter p is introduced and defined at each point as

$$p_j(t) = \frac{1}{2} \left(\frac{s_j(t)}{s_N(t)} + \Gamma_j \right) \quad \text{for } j = 0, \dots, N. \tag{12}$$

The cubic splines for p and Γ can be constructed in the same way as in Step 1. In Step 5, points $\{(x_j, y_j)\}$ redistributed with respect to the parameter p , not the arc-length s . The reason for this is given shortly.

Step 4 is the procedure of point insertion. One may apply various strategies for the point insertion. We increase the number of points by factors of $\frac{5}{4}$, $\frac{5}{4}$, and $\frac{32}{25}$ in turn as this method produces twice number of points after a 3-cycle insertion. The reasons we adopt this insertion procedure are as follows. Point insertion and redistribution generates numerical viscosity effect. Thus we apply redistribution and point insertion only when it is necessary, rather than at every time step. Next, the method generates less redistribution errors than that of double insertion, which makes twice number of points at a time. In addition, new points are needed to be a fractional-multiple of the previous points to evaluate Fourier coefficients in Fast Fourier Transformations.

In Step 5, we redistribute the points $\{(x_j, y_j)\}$ uniformly with respect to the parameter p . If the pivotal points are redistributed evenly with respect to the arc-length, a jump in Γ gradually appears at the center of the sheet as time proceeds. In fact, the circulation parameter $\Gamma(s)$ becomes very steep around the center, because the vortex strength is so large there (see Fig. 12). Therefore, Γ may have jumps around the center even for very small change of arc-length, which produces a loss of precision in the trapezoidal approximation of the integral (5). To escape from this difficulty, we adopt the different discretization of the vortex sheet by the new artificial variable p defined as above. From (12), the differences between two neighboring normalized arc-lengths and circulation parameters are bounded by

$$|S_{j+1} - S_j| \leq \frac{2}{N} \quad \text{and} \quad |\Gamma_{j+1} - \Gamma_j| \leq \frac{2}{N} \tag{13}$$

where $S_j = s_j/s_N$. Therefore, we do not see any abrupt jumps in $s(p)$ and $\Gamma(p)$ along the sheet at any time. $x(p)$, $y(p)$, and $\Gamma(p)$ are all smooth functions with respect to the new parameterization variable p , regardless of the fact that

$y = y(x)$ may no be smooth.

The resulting algorithm from Step 1 to Step 6 guarantees fourth order accuracy in time and its spatial error is bounded by the second order discretization error of the trapezoidal quadrature.

Applying the adaptive numerical method described above to the vortex sheet with $\delta = 0.3$, $\Delta s_{\text{lim}} = \frac{1}{20}$ and $\Delta t = \frac{1}{20}$, we plot the total arc-length $s(1, t)$ and the number of points multiplied by Δs_{lim} in Fig. 3. Figure 3 shows that the total arc-length indeed grows exponentially, and therefore, so does the number of discretization points to resolve the vortex sheet. The total arc-length at $t = 2$ is about 3 and is 128 at $t = 12$, so that the growth rate is about 100 times per 10 s. The number of points N is 256 up to $t = 2.8$ and reaches 12800 at $t = 12$, which shows almost the same growth rate with the total arc-length.

The non-uniform elongation of the vortex sheet is shown in Fig. 4. The numerical parameters used in Fig. 4 are same as in Fig. 3. We define the normalized arc-length as $S(\Gamma) = s(\Gamma, t)/s(1, t)$. The leftmost graph of Fig. 4 is the normalized arc-length as a function of point marker Γ at time $t = 2, 4, 6, \dots, 12$. We observe that the sheet stretches most near both ends of the sheet and contracts near the center. The upper and the lower plots in the rightmost side display the rate of stretching at the ends and the rate of contraction at the center, respectively.

4. Numerical Computation

In this section we apply the presented numerical method and perform numerical experiments to investigate dynamics

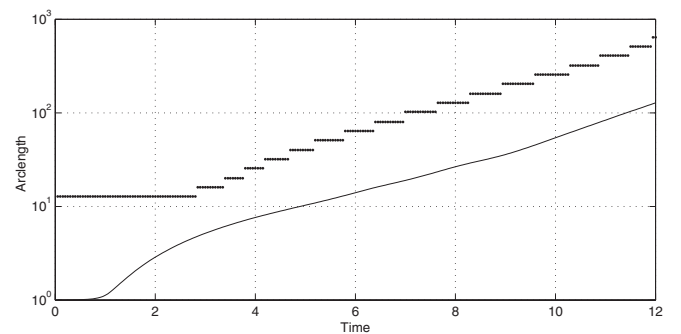


Fig. 3. Growth of the total arc-length and the number of point used for $\delta = 0.3$. The thick line shows the number of points multiplied by $\Delta s_{\text{lim}} = 1/20$.

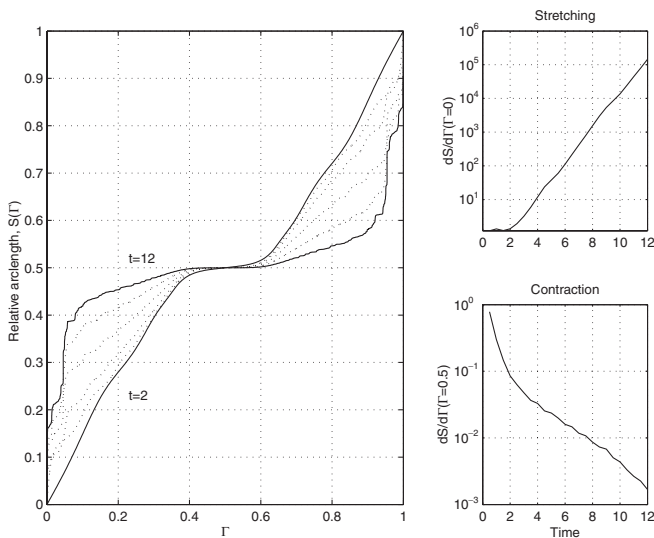


Fig. 4. Non-uniform elongation of the vortex sheet. Numerical parameters are same as Fig. 3.

of long time evolution of vortex sheet.

We first compare numerical results of the vortex sheet without and with point insertion and redistribution procedures up to time $t = 6$ in Fig. 5. For both cases, the numerical parameters are $\delta = 0.2$ and $\Delta t = \frac{1}{20}$. The value of Δs_{lim} used in Fig. 5(b) for the point insertion is $1/40$. In Fig. 5(a), the number of points are fixed to 4096 while the number of points in Fig. 5(b) is increased to 256, 512, 2048 and 3200 for $t = 0, 3, 5,$ and $6,$ respectively, by the point insertion process. Numerical results show that the computations without and with the point insertion and redistribution procedures have no difference up to time $t = 5$.

However, in spite of more points used for computation, the curve at $t = 6$ in Fig. 5(a) is tangled by large stretching at the two end points. Therefore, we conclude that the point insertion and redistribution procedures are correctly applied, not altering the dynamics of the vortex sheet.

Figure 6 illustrates the long time evolution of the vortex sheet by the point insertion and redistribution procedures up to time $t = 10$. The numerical parameters used are $\delta = 0.1,$ $\Delta t = 1/100,$ and $\Delta s_{lim} = 1/100$. The number of discretization points is $N = 256, 2048, 12800, 25600, 40960$ and 65536 for $t = 0, 3, 6, 8, 9$ and $10,$ respectively. The computation up to time $t = 10$ takes about two days using a Ultra Sparc-60 machine with a 450 MHz CPU.

Throughout the computational experiments, we find that $\Delta t = 1/20$ is sufficient for computations up to $t = 6$ as in Fig. 3 and $\Delta t = 1/100$ is suitable for $t = 10$ when the total arclength becomes about 5 times longer than that of $t = 6$. (See Fig. 10.) In fact, it would be computationally more efficient and accurate to adapt the time step proportional to the speed of vortex sheet, in order to bound movements of point vortices within fixed spatial resolution. However, the adaptive time advancing requires exponentially small time step for long time computations, since the speed of vortex sheet, as well as the arclength, increases exponentially as time goes. In our computations, we simply fix the time step Δt to $1/100,$ which is small enough to resolve the vortex sheet up to $t = 10$.

In Fig. 6, around $t = 6,$ two arms are emerging at each spiral and they start to approach to neighboring spirals. At $t = 8,$ the arms wind the spiral and the tips of arms creep into the neighboring spirals. The uniform rolling up begins to break around the outside of spirals. The curve abruptly projects up and down, which forms the shape like a bubble.

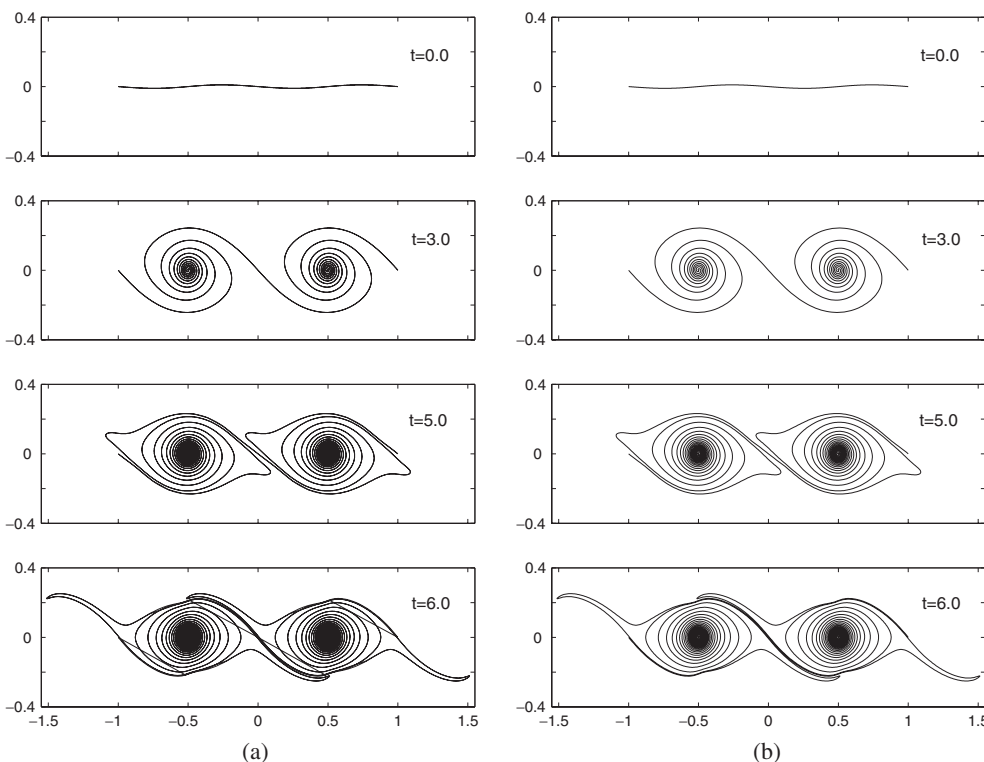


Fig. 5. Comparison for computations of the vortex sheet without/with point insertion and redistribution procedures.

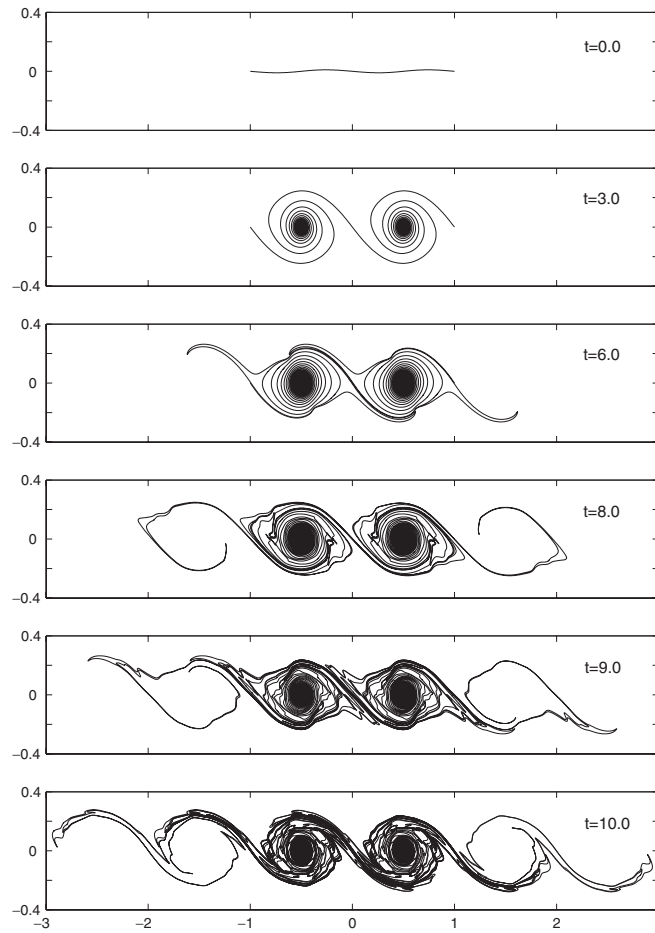


Fig. 6. Long time evolution of vortex sheet. Parameters: $\delta = 0.1$, $\Delta t = 1/100$, and $\delta s_{\text{lim}} = 1/100$.

The tips of arms are located inside this bubble shaped region. At $t = 9$, the secondary arms are formed at the first period of spirals. While these secondary arms move to the furthest stretched arms, the furthest arms are split in two branches. The tip of arms keeps migrating to the next period and the trailing part of arms is stretched to the third neighboring spirals. At $t = 10$, one branch of the trailing arms covers almost half of the third neighboring spirals and each spiral is wound by two different arms. Moreover, the roll-up of spirals is no more uniform, which leads to a very complex structure.

For a clear view, Fig. 7 magnifies the center of spiral region in Fig. 6 for $t = 3, 6, 8$ and 9 , plotting the solution on the domain $[-0.53, -0.47] \times [-0.03, 0.03]$. The curve for $t = 10$ in Fig. 6 is magnified in Fig. 8. Figure 8(a) plots the solution on the domain $[-1, 0] \times [-0.3, 0.3]$, Fig. 8(b) on the domain $[-0.3, -0.1] \times [0, 0.2]$, zooming on the right upper region of spirals, and Fig. 8(c) on the domain $[-0.6, -0.4] \times [-0.1, 0.1]$, zooming on the center of spirals. The center of spirals is again magnified in Fig. 8(d), zooming the same domain as Fig. 7. We see in Fig. 8 that the roll-up at the center keeps going on indefinitely. Figures 7 and 8 clearly shows that our numerical method of point insertion and redistribution has been successfully applied for long time computations of the vortex sheet. We obtained much more complicated fine structures of the sheet than previously published results.

Figure 9 shows the locations for vortex points on the

sheet. Figures 9(a) and 9(b) correspond to Fig. 8(b) and 8(d), respectively. We see that the resolution in our computation is good enough to describe the complex structure of the vortex sheet.

Figure 10 plots the exponential growth of total arc-length for various δ . The values of Δs_{lim} used in the computations are $1/100, 1/40$ and $1/20$ for $\delta = 0.1, 0.2$ and 0.3 , respectively. The result shows qualitatively similar growth rates for total arc-length.

Figure 11 displays the number of Fourier modes versus δ at time $t = 5$ for several values of cutoff τ . Here, the number of Fourier modes are determined by the following way. The absolute values of Fourier coefficients are fitted, in the least squares sense, by an exponential function, i.e. $|\xi(n)| \sim ae^{-bn}$ where n represents the wavenumber of Fourier modes. Then, the number of Fourier modes n are obtained by solving the equation $ae^{-bn} = \tau$. From Fig. 11, it is found that, fixing the cutoff, the number of Fourier modes increases, as δ decreases, so that the amplitudes of Fourier coefficients decay slowly. We also see that, for smaller values of cutoff, the decaying rate of Fourier modes becomes slower. This behavior is prominent especially for smaller value of δ . Therefore, the number of points required for computations drastically increases for small values of δ and cutoff τ .

Figure 12 shows the distribution of vortex strength, $d\Gamma/ds$ along the vortex sheet in Fig. 6 for several chosen times. The x -axis represents the normalized arc-length $S(\Gamma, t)$. We observe that the vorticity is concentrated only at the center

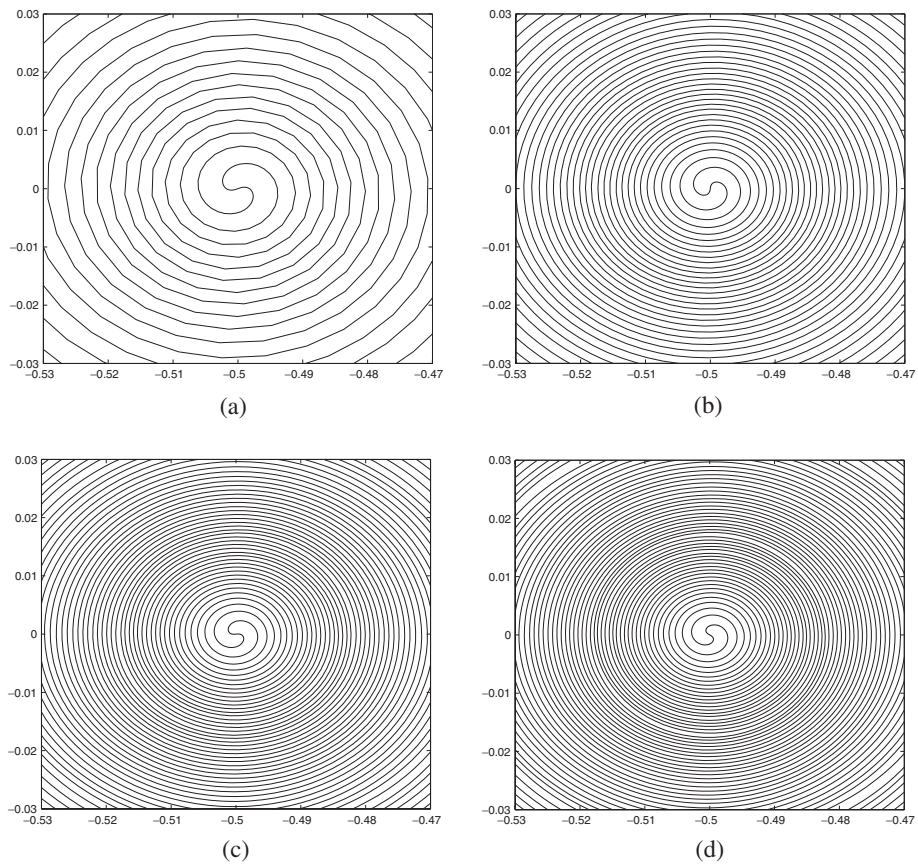


Fig. 7. Zooming of the solutions in Fig. 6. (a) $t = 3$. (b) $t = 6$. (c) $t = 8$. (d) $t = 9$.

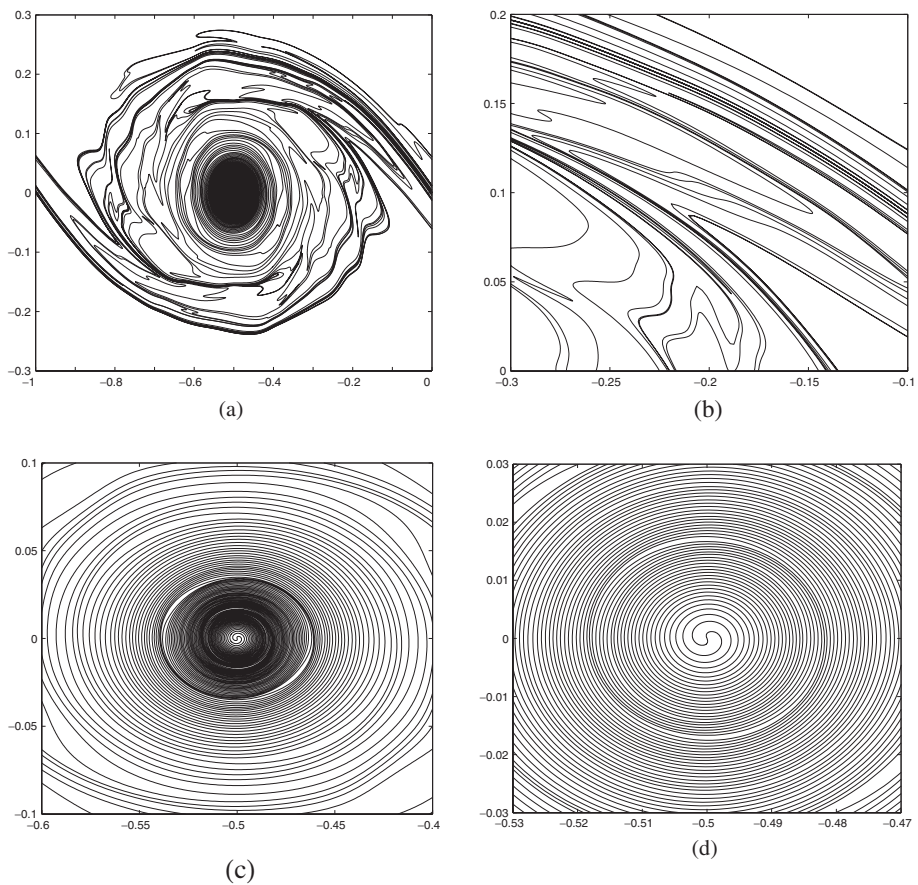


Fig. 8. Zooming of the solution at time $t = 10$ in Fig. 6.

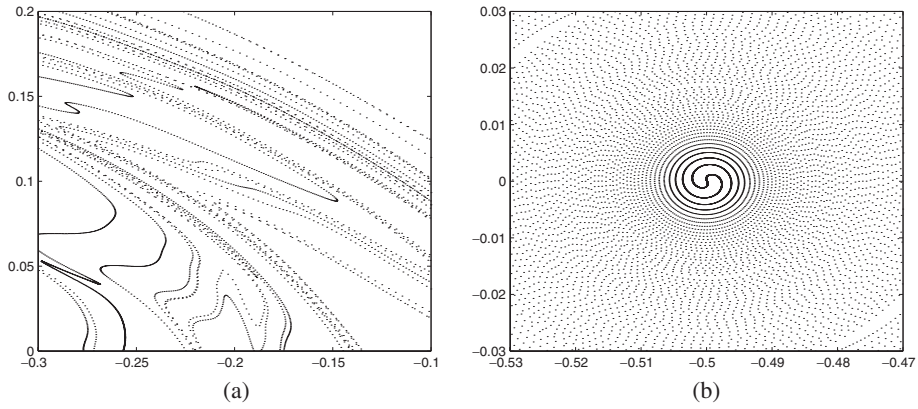


Fig. 9. Locations for vortex points on the vortex sheet. (a) and (b) correspond to Figs. 8(b) and 8(d), respectively.

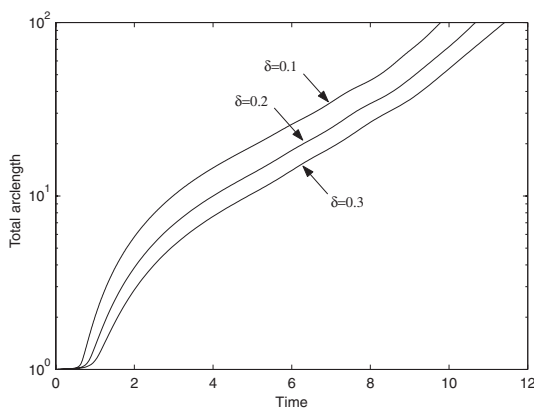


Fig. 10. Growth of total arc-length for various δ .

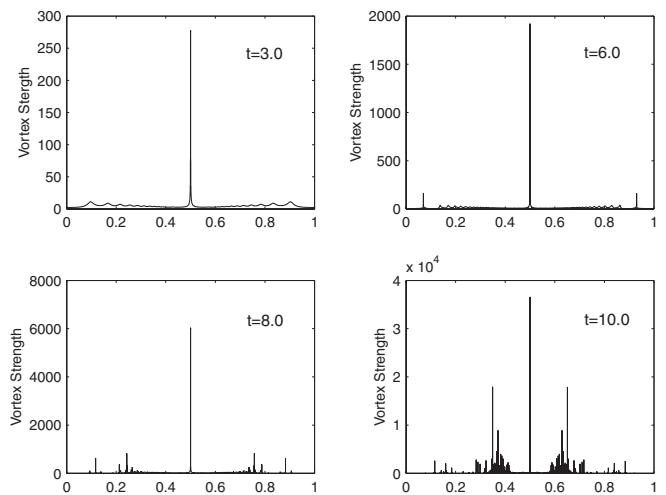


Fig. 12. Distribution of vortex strength along the vortex sheet. x -axis represents the normalized arc-length $S(\Gamma, t)$.

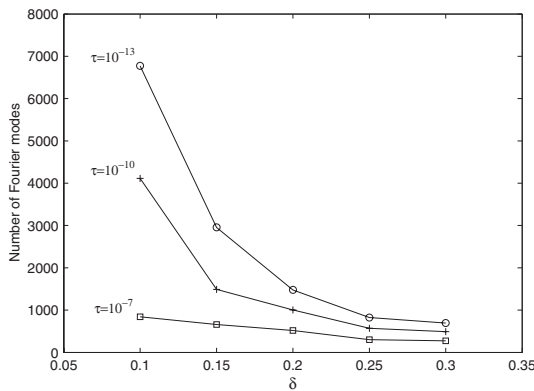


Fig. 11. Number of Fourier modes as a function of delta for various

of spirals at early times, but a number of strong vorticities are found at time $t = 10$ and values of some vorticities are even larger than that of vorticity at the center at time $t = 8$. Figure 13 is the logarithmic plot for the growth of vortex strength at the center of the vortex sheet. Similar to the case of total arc-length, the vortex strength at the center grows exponentially. The 3D surface plot of the vortex strength at $t = 10$ is given in Fig. 14.

5. Discussions

We have presented a robust and efficient point vortex method, adopting point insertion and redistribution proce-

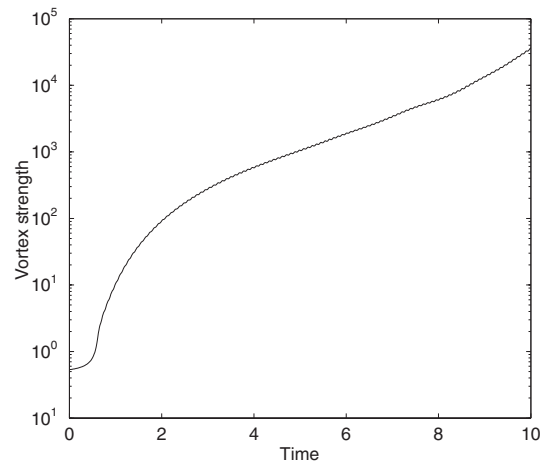


Fig. 13. Growth of vortex strength at the center of vortex sheet.

dure, to compute the long time evolution of a two-dimensional vortex sheet. The computational results show that the present method has been successfully applied to describe the dynamics of long time vortex sheet. We have checked that our method gives exactly same solutions with Krasny's results for a large value of smoothing parameter δ .¹²⁾ Compared to previously published results, the solutions

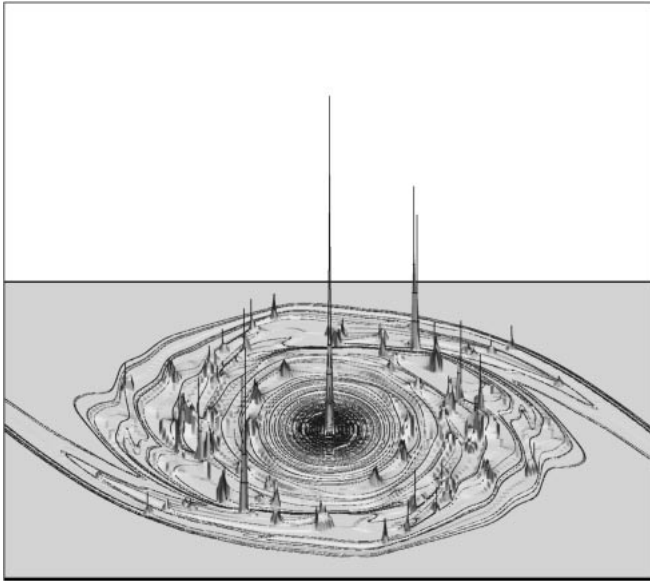


Fig. 14. Vortex strength along the vortex sheet at $t = 10$.

with fine structures of various scales are obtained.

We observe that the rolling up of vortex sheet after a very long time displays a chaotic pattern. The spiral is deformed into a non-uniform one, while it keeps rolling up. This long time behavior may suggest an emergence of chaos in the evolution of the sheet, as it is similar to the results by Krasny and Nitsche¹³⁾ for the vortex pair or vortex ring occurring in potential flow past a flat plate or a circular disk. Krasny and Nitsche simulated a long time evolution of the vortices by a similar vortex blob method to ours and found irregular pattern of the roll-up of the vortex sheet which is related to the characteristic of chaos.

The long time behavior of the vortex sheet also indicates the applicability of the Poincare recurrence theorem. Krasny remarked the applicability of the theorem for the vortex sheet, assuming that the interface is bounded in the vertical direction.¹⁰⁾ Our computational results show that the height of the vortex sheet remains bounded in long time. Therefore, the Poincare recurrence theorem's conclusion may be drawn to characterize the feature of the vortex sheet: any point on the sheet might return close to its initial position in phase

space either by rotating inside the spiral or by migrating into another period and approaching its initial coordinates shifted by an integral multiple of period in horizontal direction.

Our results also give affirmative clues to the conjecture of D. Pullin of the shape of sheet after the critical time of curvature singularity. We demonstrated that the roll-up continues as time goes on and the center of spiral is producing smaller and smaller scale turns. This result is consistent with the conjecture that the sheet is a double branched spiral with an infinite number of turns.¹⁰⁾

We believe that the numerical solution at $t = 10$ already shows fully developed structures, and the computation for much longer time requires too many number of discretization points due to the exponential and non-uniform stretching of the interface. Developing a faster and robust numerical method with high accuracy will be the next step of the research.

Acknowledgements

Kim was supported by Korea Research Foundation Grant (KRF-2001-015-DP0024), Lee by Korea Science and Engineering Foundation (KOSEF) under grant number R01-2000-00008 and Sohn by the Basic Research Program of KOSEF under grant No. R01-2000-00002.

- 1) B. R. Baker: *J. Fluid Mech.* **100** (1980) 209.
- 2) G. Baker and A. Nachbin: *SIAM J. Sci. Comput.* **19** (1998) 1737.
- 3) J. T. Beale and A. Majda: *J. Comput. Phys.* **58** (1985) 188.
- 4) G. Birkhoff: *Proc. Symp. Applied Mathematics* (AMS, Providence, 1962) Vol. XIII.
- 5) M. Brady, A. Leonard and D. I. Pullin: *J. Comput. Phys.* **146** (1998) 520.
- 6) A. J. Chorin and P. S. Bernard: *J. Comput. Phys.* **13** (1973) 423.
- 7) P. T. Fink and W. K. Soh: *Proc. R. Soc. London A* **362** (1978) 195.
- 8) J. T. Hamilton and G. Majda: *J. Comput. Phys.* **121** (1995) 29.
- 9) T. Ishihara and Y. Kaneda: *J. Phys. Soc. Jpn.* **63** (1994) 388.
- 10) R. Krasny: *J. Comput. Phys.* **65** (1986) 292.
- 11) R. Krasny: *J. Fluid Mech.* **184** (1987) 123.
- 12) R. Krasny: *Fluid Dyn. Res.* **3** (1988) 93.
- 13) R. Krasny and M. Nitsche: *J. Fluid Mech.* **454** (2002) 47.
- 14) J.-G. Liu and Z. Xin: *Commun. Pure Appl. Math.* **48** (1995) 611.
- 15) D. W. Moore: *Proc. R. Soc. London A* **365** (1979) 105.
- 16) D. W. Moore: *SIAM J. Sci. Stat. Comput.* **2** (1981) 65.
- 17) T. Sakajo and H. Okamoto: *J. Phys. Soc. Jpn.* **67** (1998) 462.
- 18) M. J. Shelley: *J. Fluid Mech.* **244** (1992) 493.